

GenVDM: Generating Vector Displacement Maps From a Single Image

Anonymous CVPR submission

Paper ID 10476

Abstract

001 We introduce the first method for generating *Vector Dis-
002 placement Maps (VDMs)*: parameterized, detailed geo-
003 metric stamps commonly used in 3D modeling. Given a single
004 input image, our method first generates multi-view normal
005 maps and then reconstructs a VDM from the normals via
006 a novel reconstruction pipeline. We also propose an effi-
007 cient algorithm for extracting VDMs from 3D objects, and
008 present the first academic VDM dataset. Compared to exist-
009 ing 3D generative models focusing on complete shapes, we
010 focus on generating parts that can be seamlessly attached
011 to shape surfaces. The method gives artists rich control
012 over adding geometric details to a 3D shape. Experiments
013 demonstrate that our approach outperforms existing base-
014 lines. Generating VDMs offers additional benefits, such as
015 using 2D image editing to customize and refine 3D details.

1. Introduction

016 Generative neural models for 3D shape synthesis is a
017 rapidly advancing research area [58]. However, they are
018 still not widely adopted in artistic workflows for two main
019 reasons. First, synthesizing fine geometric details is chal-
020 lenging due to the heterogeneity of 3D representations and
021 the lack of detailed 3D training data. Second, existing neu-
022 ral tools lack the precise spatial and compositional controls
023 needed by 3D artists. To address these limitations, instead
024 of reinventing the 3D modeling stack to accommodate gen-
025 erative AI, we draw inspiration from an existing workflow
026 in which an artist starts with a base mesh and “stamps” the
027 desired details onto the 3D surface (see Figure 1). These
028 smaller stamps are easier to generate than full-scale 3D
029 models, fit seamlessly into existing workflows, eliminate
030 artists’ dependence on expensive and limited third-party
031 stamp libraries, and provide full artistic control over spatial
032 arrangement and composition.

033 We chose the *vector displacement map* or VDM as our
034 stamp representation. A VDM assigns an arbitrary 3D dis-
035 placement to every point in a 2D rectangle, warping the
036

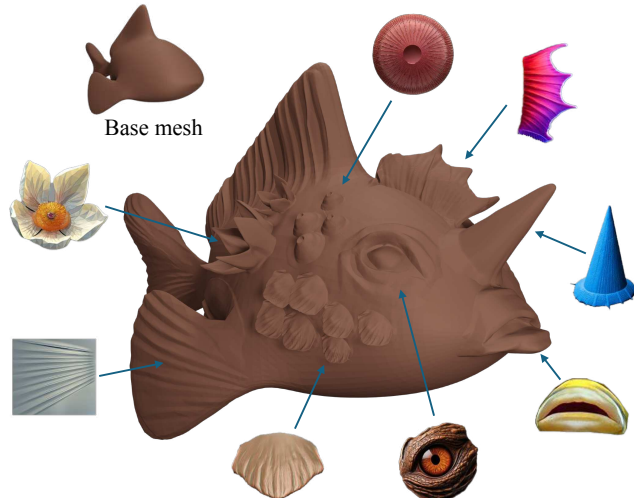


Figure 1. We introduce GenVDM, a method that can generate a highly detailed Vector Displacement Map (VDM) from a single input image. The generated VDMs can be directly applied to mesh surfaces to create intricate geometric details. Note that the thumbnails represent plain 2D RGB image sources.

037 sheet to form a curved surface with complex geometric fea-
038 tures, such as overhangs and cavities. It is widely supported
039 in 3D software [1–4] and compactly stored as a vector field
040 over a UV image domain. While using VDMs is common-
041 place, authoring them is extremely challenging, and artists
042 usually depend on packs of VDMs created by third parties
043 (analogous to brushes in digital painting tools), with lim-
044 ited customization or generality. Image or text-driven stamp
045 generation could drastically expand the scope of VDM us-
046 age by providing artists with custom stamps on demand.

047 In this paper, we propose the first neural pipeline to gen-
048 erate a VDM from a single RGB image. To achieve this,
049 we address two main technical challenges. The first chal-
050 lenge is that existing generative models are not suitable for
051 VDM generation: generating a 3D object usually does not
052 also produce a parametric 2D domain for stamp applica-
053 tion, and predicting a depth map from a single image does
054 not capture complex high-amplitude variations, overhangs,
055 and occlusions; see Figure 6. Thus, we develop a three-step
056 method. First, given an input RGB image (which can also

057 be generated with existing text-to-image models), we pre-
058 dict normal maps from multiple viewing directions to re-
059 solve occlusions that may be hidden in a single view. Sec-
060 ond, we reconstruct a mesh (which need not have disk topol-
061 ogy) by fitting a neural SDF to the multi-view normal maps
062 and polygonizing the result. Third, we use a neural de-
063 formation model to displace points on a 2D rectangle to fit the
064 mesh, forming the final VDM.

065 The second challenge in training a generative VDM
066 model is the absence of training data. We tackle it by build-
067 ing an interactive tool to segment interesting semantic and
068 geometric regions from Objaverse 3D models [19], and then
069 develop a geometry processing pipeline for converting these
070 regions into a VDM representation, creating a dataset of
071 1,200 VDM patches used for training. Our pipeline is ro-
072 bust enough to analyze polygon soups in the wild, which
073 we achieve by re-sampling the selected regions and recon-
074 structing a single connected surface after removing outliers.
075 We then deform the resulting mesh to obtain a co-planar
076 boundary that can be seamlessly attached to a flat base tile
077 over which the VDMs are typically defined. The processed
078 shapes can then be rendered and used to finetune the multi-
079 view normal generation model.

080 We compare our method to state-of-the-art shape gener-
081 ation techniques [27, 40, 51], as well as to reconstructing
082 a heightfield (i.e. a *scalar* displacement map) from esti-
083 mated depth [81]. We use a collection of images depicting
084 parts commonly used in VDMs (e.g., facial elements, dec-
085 orations), and evaluate using visual fidelity [54] and seman-
086 tic similarity [52] metrics. Our method outperforms others
087 due to its ability to handle smaller VDM-like regions. Note
088 also that other mesh generation methods do not produce a
089 displacement map – which can have both “outward” and
090 “inward” displacements – and thus their output can only be
091 additively combined with the base shape, e.g., they are not
092 able to introduce cavities like an eye or a mouth in Figure 1.

093 To summarize, our contributions are:

- 094 • The first generative ML pipeline for VDMs;
- 095 • A robust method to reconstruct VDMs from multi-view
096 normal maps produced by image diffusion models;
- 097 • A novel VDM extraction pipeline to efficiently extract
098 and process patches from 3D objects to produce VDMs;
- 099 • The first public dataset of VDMs for academic research.

100 2. Related work

101 **Vector Displacement Maps.** Texture mapping [10, 26] is
102 the dominant solution in the industry to add complex sur-
103 face details to shapes without increasing mesh complexity.
104 Accompanying it are many techniques that hallucinate com-
105 plex geometric details, such as bump mapping [9], horizon
106 mapping [43], and parallax mapping [30]. Unlike those
107 techniques that do not change the geometry of the shape,

108 displacement mapping [17, 18, 61] adds geometric details
109 by subdividing the original geometry into finer polygons
110 and then displacing each vertex in its normal direction by a
111 height value indexed from the displacement map (although
112 some versions of displacement mapping can be done in the
113 pixel space without changing the original geometry [66]).

114 While a displacement map can be considered as a single-
115 channel image or heightfield, a vector displacement map
116 (VDM) can be seen as a three-channel image, where each
117 pixel contains a 3D displacement vector. VDMs naturally
118 support representing more complex geometries with less
119 distortion compared to displacement maps, and both are
120 used in 3D modeling tools to create geometric details. Re-
121 search on displacement maps and VDMs has focused on
122 texture synthesis from examples [82], and synthesis of hu-
123 man body and face meshes for shape reconstruction [6, 80].
124 VDMs conceptually resemble Geometry Images [23], and
125 some recent works adopt image diffusion models for gener-
126 ating Geometry Images to synthesize 3D shapes [20, 79].
127 To our knowledge, there is no prior work on generative
128 models of VDMs, nor a public research dataset for VDMs.

129 **Image-to-3D.** Early works on single-view 3D reconstruc-
130 tion [15, 16, 22, 45, 67, 78, 83] mostly adopt feed-forward
131 neural networks trained on limited data [11]. More recent
132 work [29, 46, 85, 87] trained on large 3D datasets [19]
133 has shown significantly improved generalizability to novel
134 shape categories. With the introduction of text-to-image
135 diffusion models [49, 53], a line of work [44, 63] achieved
136 zero-shot single-image-to-3D with score distillation sam-
137 pling (SDS) [50] by distilling 2D diffusion priors into 3D
138 representations with per-shape optimization.

139 Another line of work [38, 71] utilizes image diffusion
140 models for novel view synthesis conditioned on an input
141 image and a relative camera pose. Such models produce
142 images of the object from different views, therefore the
143 3D object can be reconstructed by SDS-based optimiza-
144 tion [38, 51] or a feed-forward reconstruction network [37].
145 These methods inspired a series of subsequent work that
146 finetunes pretrained image diffusion models to directly gen-
147 erate 3D-consistent multi-view images of the target out-
148 put shape given a single-view image, where the output
149 shape can be reconstructed from generated multi-view im-
150 ages via optimizing a neural field or mesh [39, 40, 57],
151 a 3D diffusion reconstruction network [36], or a feed-
152 forward large reconstruction model powered by Transfor-
153 mers [27, 34, 64, 68, 70, 72, 74, 76, 86, 88]. Most recently,
154 image diffusion models have been replaced by video diffu-
155 sion models to achieve better 3D consistency of the gener-
156 ated views [24, 65].

157 **Modeling by Parts.** The use of small building compo-
158 nents to compose complex shapes has been widely studied
159 in modeling-by-assembly systems [21, 32]. Before gener-

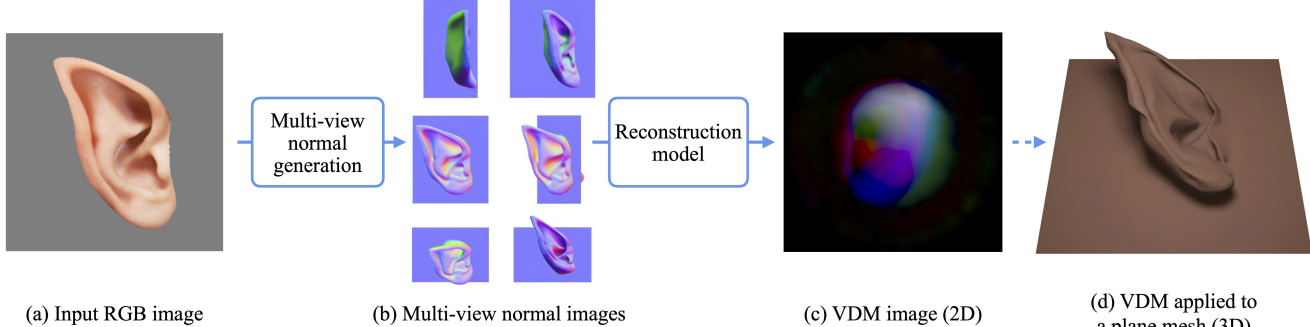


Figure 2. Overview of our image-to-VDM pipeline. Given an input image, we first add a gray square behind the object/part in the image as background, so the image resembles a textured VDM applied to a square mesh, as in (a). Then we utilize a multi-view image diffusion model to generate six normal maps with pre-defined camera poses, as in (b). The multi-view normal maps effectively represent the geometry of the VDM when applied to a square mesh, and thus we can reconstruct the VDM from these normal maps, as in (c). The reconstructed VDM can then be applied to various surfaces as in (d).

160 active AI rose to prominence, these systems relied on part
 161 databases [12] (or shape databases from which parts could
 162 be cut out), and focused on building tools to help users find
 163 the right parts [7, 13, 56, 75] and assemble them meaning-
 164 fully [28, 60, 77]. As a variation, methods were developed
 165 to extract and transfer detailed patches from a shape to an-
 166 other [62]. A few papers studied joint synthesis and layout
 167 of parts [35], but the synthesis was conditioned only on the
 168 layout and not on user input, and the focus was on whole-
 169 shape generation and not adding detail to existing ones.

170 Relying on existing part datasets or part generation with-
 171 out user control, and on complex, non-standard, topology-
 172 sensitive mesh fusion algorithms limits the utility of these
 173 older methods. Our approach generates detailed comple-
 174 mentary geometry in-situ from the image prompt, and our
 175 generated VDMs are defined over parameterized 2D do-
 176 mains which are suitable for seamlessly blending onto 3D
 177 models, with industry-wide support.

178 3. Method

179 Our image-to-VDM pipeline is shown in Figure 2. Similar
 180 to other methods in the literature, we follow an approach
 181 that first generates multi-view images of the target object
 182 with an image diffusion model and then reconstructs the
 183 object from the generated images. In particular, we only
 184 generate normal maps of the object as we are only interested in
 185 the geometric details. Details of the multi-view normal gen-
 186 eration are described in Section 3.1. Next, we reconstruct
 187 the VDM from the multi-view normals. As VDMs have
 188 specific properties and constraints, reconstructing them is
 189 highly non-trivial. We report our attempts and solutions
 190 in Section 3.2. Finally, as there is no publicly available
 191 dataset for VDMs, we designed an efficient tool for extract-
 192 ing shape patches from Objaverse [19], and devised algo-
 193 rithms to process those patches for use as training data. We
 194 describe the data processing pipeline in Section 3.3.

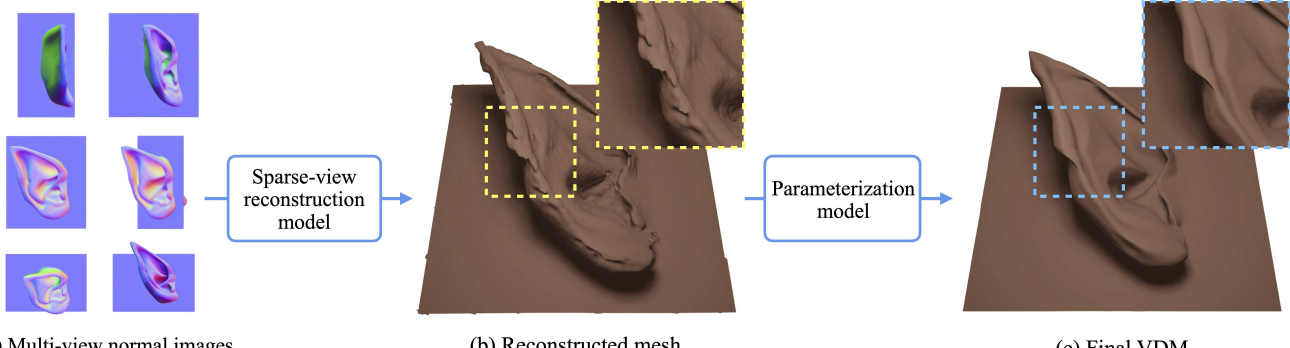
195 3.1. Multi-View Normal Map Generation

196 We opt to finetune an image diffusion model to generate
 197 multi-view images, as the pretrained image diffusion model
 198 offers strong generalizability. As will be shown in our ex-
 199 periments, our model, trained on a small dataset of 1,200
 200 examples, works on a large variety of shapes.

201 Specifically, we adopt Zero123++ [57] as the back-
 202 bone for our multi-view diffusion model. Zero123++ is an
 203 image-to-multiview model based on Stable Diffusion [53].
 204 Given an input image, Zero123++ generates a 960×640
 205 image representing six multi-view images in a 3×2 grid,
 206 where the six images have pre-defined camera poses so they
 207 can be easily used for 3D reconstruction. However, the pre-
 208 defined camera poses in Zero123++ fully surround the ob-
 209 ject, e.g., there are front views and back views of the object.
 210 In our pipeline, since we are aiming to generate VDMs, the
 211 back views of the object are unnecessary. Therefore, we
 212 re-designed the camera poses of the six images. As shown
 213 in Figure 2 (b), assuming the front view (see (a) for an ex-
 214 ample) has (elevation angle, azimuth angle) = $(0^\circ, 0^\circ)$, we
 215 define the six camera poses to be $(0^\circ, -60^\circ)$, $(0^\circ, -30^\circ)$,
 216 $(0^\circ, 30^\circ)$, $(0^\circ, 60^\circ)$, $(45^\circ, 0^\circ)$, $(-45^\circ, 0^\circ)$. We also adopt
 217 orthographic cameras to reduce distortion, and let the model
 218 generate a normal map of the object for each camera pose.
 219 To train the model, we render single-view RGB images as
 220 input and multi-view normal maps as ground truth output.
 221 Details about training data is described in Section 3.3. Note
 222 that the input image does not have to be a front view; we
 223 render random views for training so the model can handle
 224 images from various viewpoints. We finetune on the check-
 225 point provided by Zero123++ [57] on 8 NVIDIA A100
 226 GPUs for 3 days.

227 3.2. VDM Reconstruction

228 Reconstructing 3D shapes from multi-view images has been
 229 well studies in the text/image-to-3D literature. Most recent



(a) Multi-view normal images

(b) Reconstructed mesh

(c) Final VDM

Figure 3. Reconstructing VDM from multi-view normal maps. We adopt a two-step approach. First, we reconstruct an accurate (but perhaps noisy) mesh (b) from the multi-view normals (a) with differentiable rendering and neural SDF representation. Then we parameterize the mesh by fitting a deformable square to it with a neural deformation field, as in (c). An VDM image can thus be obtained by discretizing the square into pixels and infer each pixel's displacement from the neural deformation field. The whole reconstruction pipeline takes about 6 minutes for each shape on an NVIDIA A100 GPU, where each step takes about 3 minutes.

230 methods adopt a feed-forward large reconstruction model
231 (LRM) to directly generate a 3D shape from multiple input
232 images of different viewpoints [27, 34, 64, 68, 72, 86].
233 Therefore, a straightforward way for reconstructing VDMs
234 is to train a similar LRM to take the normal maps as input
235 and directly regress a VDM image. However, given limited
236 VDM training shapes, our LRM trained on a small dataset is
237 unlikely to generalize as well as other LRM models trained
238 on larger datasets, therefore leading to suboptimal results.

239 Given the discussions above, we adopt a slower but more
240 robust per-shape optimization approach. Given the six normal
241 maps with pre-defined fixed camera poses, we want to
242 optimize a 3D representation to converge to the target 3D
243 shape with supervision provided by differentiable rendering.
244 A naive approach would be to initialize with a dis-
245 cretized square mesh and optimize with mesh-based differ-
246 entiable rendering. However, as has been shown in other
247 methods [33, 47], differentiable rendering on meshes is of-
248 ten problematic and requires careful design of regulariza-
249 tion losses and tuning of hyperparameters. As we will show
250 later, even with ground truth 3D supervision, optimizing a
251 discretized mesh to fit the target shape is not an easy task.

252 Therefore, we devise a two-step approach, as shown in
253 Figure 3, to first optimize a neural SDF field to recon-
254 struct a 3D shape from the multi-view normal maps, and then
255 parameterize the 3D shape into a VDM image. We utilize
256 the method proposed in Wonder3D [40] for the first step,
257 with the only modification being that we removed L_{rgb} , the
258 loss term to punish the difference between rendered RGB
259 images and the ground truth, as we do not predict multi-
260 view RGB images. Since we always put a grey square as
261 background in our input images, the shape we obtained via
262 optimization has a solid plane-like primitive where the
263 object/part is attached to, see Figure 3 (b); then we can extract
264 a mesh from the neural SDF field and easily separate a sin-
265 gle layer of mesh that represents the VDM.

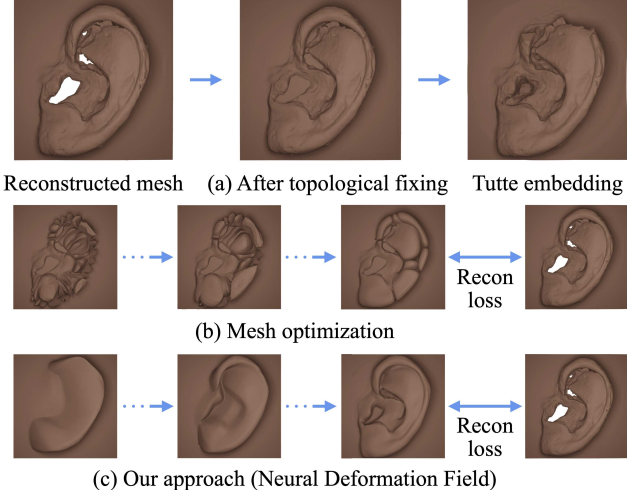


Figure 4. Comparison of different approaches for parameterizing a shape into VDM. (a) Topology fixing and Tutte embedding with classic tools leads to noise and distortion. (b) Fitting a plane mesh to the target mesh leads to large distortion. (c) Our approach by applying a neural deformation field to a parametric square leads to clean and high-quality reconstruction.

266 The next step is to parameterize the mesh into a VDM
267 image. Since the mesh is reconstructed from sparse-view
268 images, its geometry is often noisy and riddled with small
269 holes and large gaps, see Figure 4 (a) left. To convert it
270 into a VDM, we will need to fix its topology so that it is
271 topologically equivalent to a plane; and then we will apply
272 a mesh parametrization method to obtain its Tutte embedding
273 on a square, so that each pixel on the square can be
274 assigned with a displacement vector. However, as shown
275 in Figure 4 (a), although the state-of-the-art topology fixing
276 algorithms [84] can fix the topology, the result is often not
277 satisfactory, e.g., a gap that should have been filled is be-
278 ing cut, see Figure 4 (a) middle where the helix of the ear
279 is cut in half. As a result, after applying [55] to obtain its

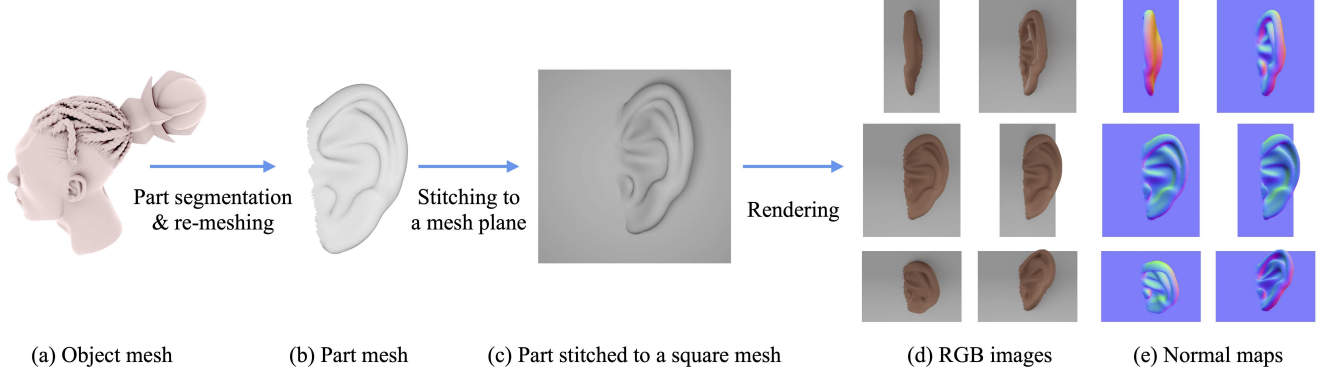


Figure 5. Data preparation. For each interesting object (a), we use a 3D lasso tool to segment out interesting parts. For each part, we densely sample points on the part’s surface and then perform Screened Poisson Surface Reconstruction [31] to obtain a single connected mesh (b). We then stitch the mesh to a square mesh with an algorithm inspired by Poisson Image Editing [48] (c). Afterwards, we can color the part and render RGB images (d) and normal maps (e) for training the image diffusion model.

embedding on a plane, we see large distortions and noise in the final VDM, see Figure 4 (a) right where the upper part of the ear is missing due to distortion.

An alternative is to initialize with an optimizable square mesh, and optimize it using a reconstruction loss with respect to the target mesh, as shown in Figure 4 (b). However, as mentioned, it is often required to have carefully designed regularization losses when a mesh is to be optimized. When adopting a naive optimization method proposed in [14], the resulting mesh exhibits large distortion.

Therefore, instead of tuning the mesh optimization algorithm, inspired by AtlasNet [22] and Deep Geometric Prior [73], we propose to deform the square mesh with a neural deformation field parameterized by a Multilayer Perceptron (MLP). The MLP acts as a natural regularizer, as its inductive smoothness bias encourages smoothness of the deformation. We define the square to be $\{p \mid p \in [0, 1]^2\}$, and the MLP ϕ_θ with optimizable parameters θ . Then, given any 2D point p in the square, we obtain its corresponding 3D point $p' = \phi_\theta(p)$ in the deformed shape. Therefore, for each optimization step, we sample a grid of 2D points in $[0, 1]^2$, apply ϕ_θ to obtain the deformed 3D points, and then compute the symmetric Chamfer Distance between the deformed 3D points and the ground truth points sampled from the target mesh. We also include a loss to maintain square boundary. Therefore our optimization objective is

$$\begin{aligned} \operatorname{argmin}_\theta \mathbb{E}_{P, Q} & \frac{1}{|P|} \sum_{p \in P} \min_{q \in Q} \|\phi_\theta(p) - q\|_2^2 + \\ & \frac{1}{|Q|} \sum_{q \in Q} \min_{p \in P} \|\phi_\theta(p) - q\|_2^2 + \\ & \frac{1}{|\partial P|} \sum_{p \in \partial P} \|\phi_\theta(p) - \text{proj}(p)\|_2^2, \end{aligned} \quad (1)$$

where P and Q are sets of sampled points from $[0, 1]^2$ and the target mesh, respectively. ∂P contains all the boundary

points in P and $\text{proj}(p)$ maps p to a corresponding 3D point in a pre-defined square boundary. After optimization, we can sample a regular grid of points in $[0, 1]^2$ and compute their 3D displacement vectors from ϕ_θ to obtain the VDM image, as shown in Figure 4 (c).

3.3. Data Preparation

To the best of our knowledge, there is no publicly available dataset for VDMs. Therefore, we developed a data processing pipeline so we can efficiently annotate interesting parts from objects and then convert the parts into VDMs. In fact, our data processing pipeline does not produce true VDMs, but rather, shapes that look like VDMs, which are good enough for training our multi-view generation model, see Figure 5. If needed, our VDM reconstruction method in Section 3.2 can be used to obtain readily usable VDMs.

To construct our VDM training dataset, we crop parts from the Objaverse [19] dataset. We first create a keyword filtering list and apply the filter on Objaverse shape captions [41, 42]. As VDMs are mostly used to model organic parts, we select objects likely to contain such parts, e.g., animals and characters.

We then developed a UI to precisely crop a part from a 3D object. This is achieved by a 3D lasso tool, where the user only needs to select a ring of points along the cutting boundary of the desired part. Our algorithm connects the points to form a cut and extracts the part from the object. Note that the part may not be a single connected mesh – it may comprise several sub-meshes. Hence, we remesh the part into a single connected mesh. We first densely sample points on the part, and then remove interior points by computing winding numbers [8]. For the remaining points, we perform Screened Poisson Surface Reconstruction [31] to obtain a single connected mesh (Figure 5 (b)). Our 3D lasso tool has proven to be quite efficient. Annotating our entire dataset with 1,200 parts took only 24 man-hours.

344 After obtaining the parts, we will then stitch each part to
345 a square mesh to mimic the appearance of a VDM applied
346 to a plane. Note that in almost all cases, the vertices on the
347 boundary of each part are not coplanar, therefore additional
348 steps are required to make them coplanar. We first deter-
349 mine the plane via least squares plane fitting with respect to
350 the boundary vertices. Then we project the boundary ver-
351 tices to the plane, and adopt a method similar to Poisson
352 Image Editing [48] to deform the part so that it follows the
353 new coplanar boundary. Denote the set of all boundary ver-
354 tices in the part (before projection) as B and non-boundary
355 vertices as A ; also denote the set of all edges as E . De-
356 note the coplanar boundary vertices after projection as B' ,
357 and the non-boundary vertices after deformation as A' . For
358 each point p in A or B , denote its corresponding point in A'
359 or B' as p' . Then our new vertices after mesh deformation
360 can be obtained by solving a quadratic error function

$$\underset{A'}{\operatorname{argmin}} \mathbb{E}_{(p,q) \in E} \|(p' - q') - (p - q)\|_2^2. \quad (2)$$

361 The minimization objective is to ensure that the gradients
362 on the mesh are preserved as much as possible after defor-
363 mation, while the target coplanar boundary points B' are
364 also strictly followed.

365 We then place the deformed part on a square mesh so
366 that the boundary vertices and the square mesh vertices are
367 coplanar. Once the part is attached to the square mesh, we
368 perform one additional Laplacian Smoothing step to the ver-
369 tices close to the boundary to remove boundary noise, see
370 Figure 5 (c). We always keep the square mesh gray and
371 assign a random color to the part. We also performs transla-
372 tion, scaling, and rotation augmentation to the part to enrich
373 the diversity of the dataset. Finally, for each shape, we ren-
374 der several RGB images from different viewpoints to serve
375 as the training input to the multi-view normal generation
376 model, and six normal maps in pre-defined camera poses as
377 the ground truth output, see Figure 5 (d, e).

379 4. Experiments

380 In this section, we verify the effectiveness of our method
381 by comparing it with various state-of-the-art methods. We
382 also validate our design choices in ablation studies. Fi-
383 nally, we present additional results produced by our method,
384 show applications of VDMs on adding details to geometry,
385 and demonstrate how users can customize VDMs by simply
386 editing the input images. We will make our code, trained
387 model weights, and dataset available to the public.

388 4.1. Vector Displacement Map Generation

389 **Baselines.** Since there is no prior work on generating
390 VDMs from single view images, we compare our method
391 with methods that perform a similar task, namely, single-
392 view image to 3D reconstruction. Specifically, we compare

393 our method with Wonder3D [40], Magic123 [51], Large Re-
394 construction Model (LRM) [27], as well as a *scalar* dis-
395 placement map (scalar DM) reconstruction method based
396 on DepthAnything [81]. Given an input image, Won-
397 der3D [40] generates multi-view RGB and normal images
398 and optimizes a neural SDF field to reconstruct the 3D
399 shape from the multi-view images. Magic123 [51] lever-
400 ages SDS loss [50] to optimize the 3D shape while apply-
401 ing a reconstruction loss on the input view. LRM [27] gener-
402 ates multi-view RGB images and trains a Transformer-
403 based feed-forward model to reconstruct the 3D shape from
404 the multi-view images. To validate the necessity of gener-
405 ating *vector* displacement map instead of regular *scalar*
406 displacement map, we also compare with a state-of-the-art
407 depth prediction method, DepthAnything [81], by convert-
408 ing the predicted depth of the object into a *scalar* DM.
409 We run these baseline models with official implementa-
410 tion and pretrained weights; except that LRM does not release
411 the official code, so we use open-source implementation
412 OpenLRM [25] instead. For all the reconstructed shapes,
413 we render textureless images for visualization and evalua-
414 tion. For Wonder3D, Magic123, and LRM, as they generate
415 complete objects and not VDMs, we put a square plane be-
416 hind their generated shapes to make the visualization more
417 consistent and to have a fair quantitative comparison.

418 **Evaluation Dataset and Metrics.** As there is no exist-
419 ing benchmark dataset for VDMs, we collected a dataset
420 of 50 RGB images from the Internet and a text-to-image
421 model [5] for evaluation. All images depict common VDM
422 categories used by artists such as facial elements and dec-
423 orations. For quantitative evaluation, we measure CLIP sim-
424 ilarity [52] and 3D-FID score [69] between the input im-
425 age and the rendered images of the generated shapes from
426 different views, denoted as **CLIPImg** and **3D-FID**, respec-
427 tively. For CLIP, we additionally evaluate semantic align-
428 ment by measuring CLIP similarity between the rendered
429 images and the texts describing the categories of the input
430 images, denoted as **CLIPText**. We use public implemen-
431 tation of CLIP [59] and 3D-FID [54] for computing the met-
432 rics. Please see Supplementary Material for more details.

433 The quantitative results are summarized in Table 1 and
434 qualitative results are presented in Figure 6. Quantitatively,
435 our method outperforms others by a significant margin. The
436 closest competitors to our method are Wonder3D and scalar
437 DM, which is also reflected in the qualitative results in Fig-
438 ure 6. Magic123 and LRM lack geometric detail as they rely
439 heavily on textures which often hallucinate details in geo-
440 metry. Wonder3D has a similar shape generation pipeline
441 with ours, yet it was designed to generate complete objects.
442 Therefore, it struggles to generate partial shapes, e.g., noses
443 and ears. Although the results of scalar DM look reason-
444 able from the front view, its side view suffers as scalar DM
445 cannot represent unseen regions of the front view.

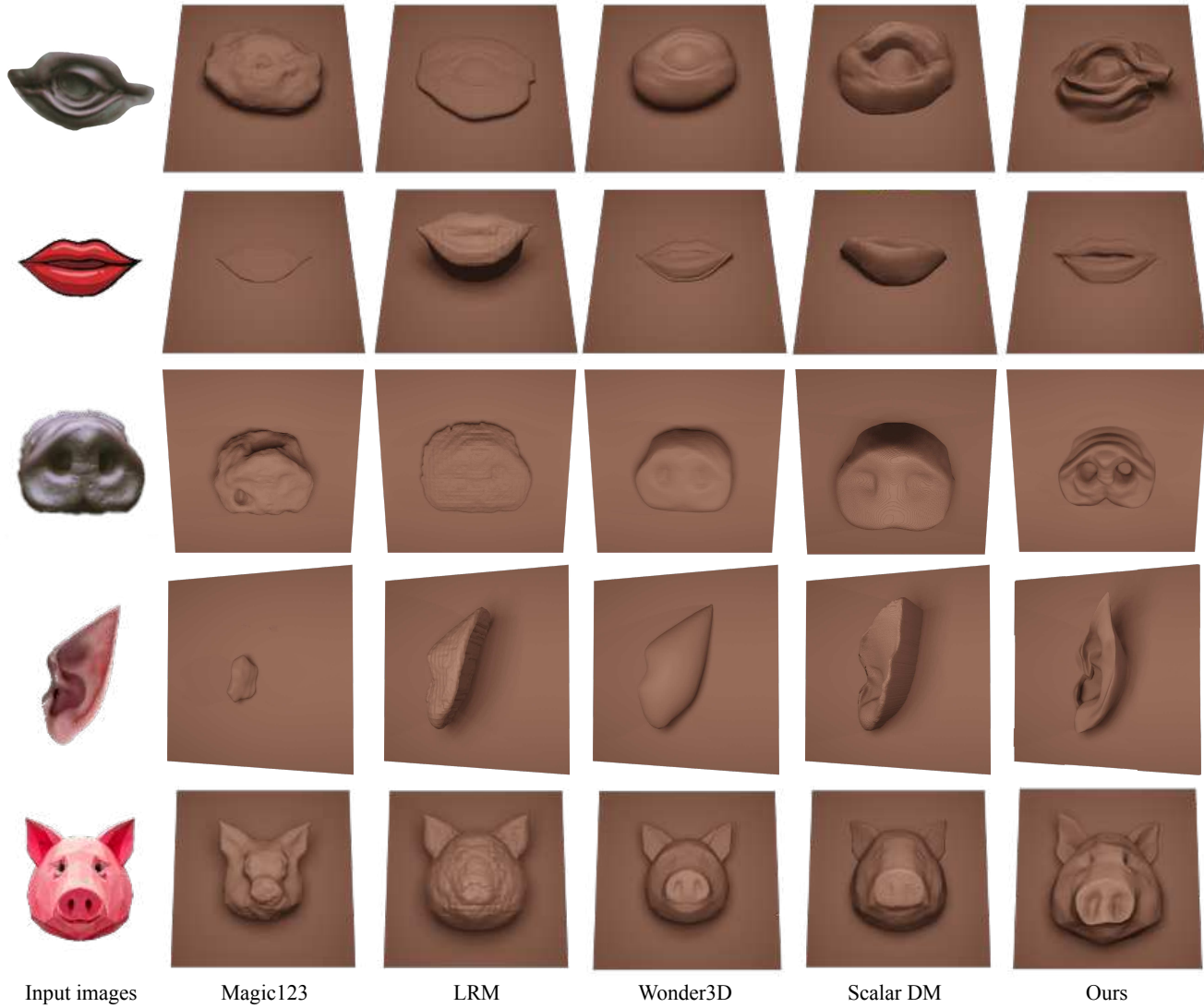


Figure 6. Qualitative results compared with baseline methods. As Magic123 [51], LRM [27], and Wonder3D [40] generate complete objects and not VDMs, we put a square plane behind their generated shapes to make the visualization more consistent.

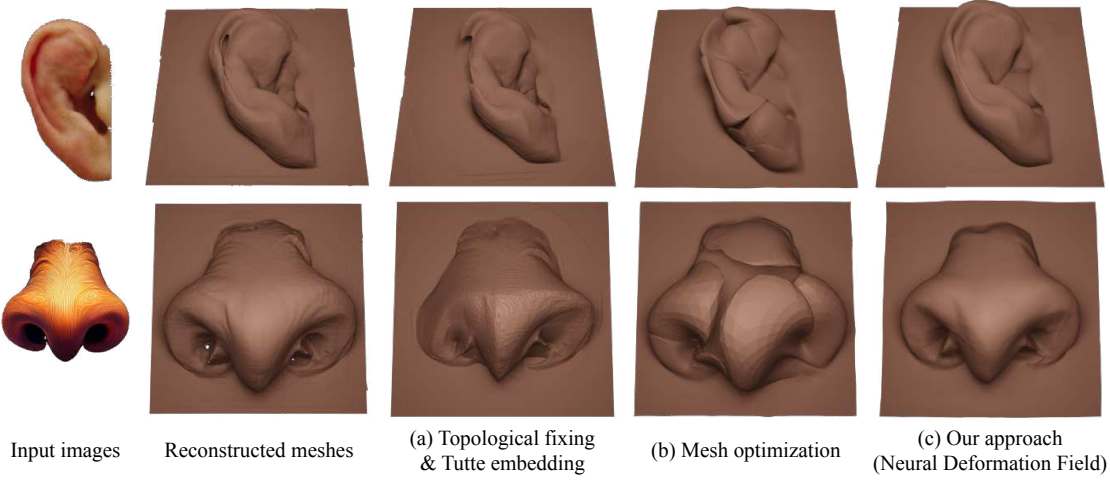


Figure 7. Qualitative results of ablation study.

Method	CLIPImg↑	CLIPText↑	3D-FID↓
Wonder3D [40]	0.8246	0.2542	199.5
Magic123 [51]	0.8293	0.2510	213.2
LRM [27]	0.8144	0.2510	239.9
Scalar DM	0.8223	0.2564	213.0
Ours	0.8520	0.2701	192.7

Table 1. Quantitative comparison with baseline methods. Scalar DM stands for scalar displacement map produced from DepthAnything [81].

Method	CLIPImg↑	CLIPText↑	3D-FID↓
Recon. Mesh	0.8440	0.2636	198.0
Topo. Fix(a)	0.8401	0.2617	209.9
Mesh Opt.(b)	0.8245	0.2525	217.2
Ours(c)	0.8521	0.2701	192.7

Table 2. Quantitative ablation on VDM Reconstruction.

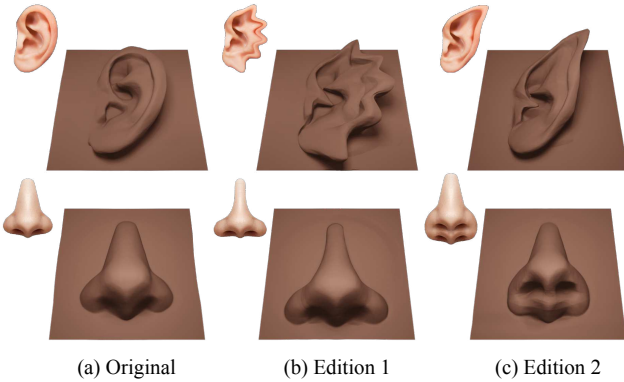
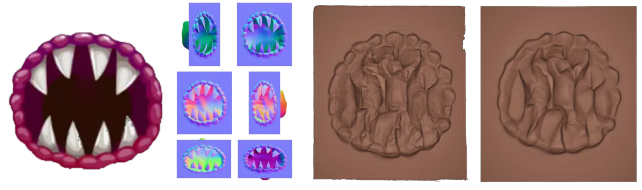


Figure 8. Customizing VDMs by editing images. Here we show original input images and generated VDMs in (a) and edited images and their generated VDMs in (b)(c).

446

4.2. Ablation Study

As discussed in Section 3.2, we compare the following settings for parameterizing the reconstructed mesh into a VDM image: (a) Topology fixing and Tutte embedding, (b) fitting a square mesh into reconstructed mesh, and (c) our approach; see Figure 4. We also include the reconstructed mesh before parameterization as a reference baseline. Table 2 summarizes quantitative results and Figure 6 shows qualitative comparisons. Topological fixing and Tutte embedding suffer when the topology of the reconstructed mesh is complex due to noisy reconstruction results, as shown in Figure 6 (a). This is because the topological fixing algorithm does not consider the distortion after parameterization as one of its optimization goals, thus some topological fixes may significantly increase distortion. Figure 6 (b) shows that mesh optimization is not reliable in our setting, and is likely to fall into local minima during optimization. In contrast, our method, shown in Figure 6 (c), not only reconstructs high quality VDMs with correct topology, but also smooths out noise induced in neural SDF reconstruction, leading to visually more pleasing results.



(a) Input image (b) Normal maps (c) Reconstructed mesh (d) Final VDM

Figure 9. Failure case.

4.3. Application

Shape modeling. With our method, users are able to generate parts of the shape from single-view images or text prompts (via text-to-image to obtain the input to our method). Compared with methods that generate complete shapes, our method naturally provides more controllability, as users can start with a coarse shape and add customization details and shape parts, see Figure 1. We also show a video in the Supplementary Material to demonstrate the modeling process with VDMs generated by our method.

Part editing. With our image-to-VDM, one can perform editing in 2D image space and change the appearance of the part in 3D, see Figure 8. Editing in image space is typically much more convenient than sculpting 3D shapes, therefore allowing users to customize their parts with ease.

5. Conclusion, Limitation, and Future Work

In this work, we propose a method to generate a VDM from an input single-view image. Our method first finetunes a pretrained image diffusion model to generate multi-view normal maps from the input image, and then reconstructs a VDM image from the multi-view normals. The generated VDMs can be used directly in shape modeling, which provide more freedom to the users on the appearance and position of each part on the shape. We also propose an efficient pipeline for creating a VDM dataset from 3D objects. Our method outperforms state-of-the-art image-to-3D models and scalar displacement map baseline, proving that our approach is more suited for VDM generation.

As discussed in Section 3.2, our VDM reconstruction involves per-shape optimization, making its inference time significantly slower than the current image-to-3D methods with feed-forward LRM. Investigating the possibility of a VDM-LRM with limited training data is of great interest to us. For certain shapes with thin structures, our method cannot produce plausible results, while the generated normals look reasonable, see Figure 9. We suspect it is due to the multi-view images being inconsistent across different views, as observed by many other works [24, 65].

VDMs are predominantly used for modeling organic shapes, yet the idea of modeling-by-parts can be applied to the majority of 3D shapes. There are exciting further avenues for part-based 3D generative models.

509

510

References

[1] Blender. vector displacement node. https://docs.blender.org/manual/en/latest/render/shader_nodes/vector/vector_displacement.html. 1

[2] Maya. vector displacement - arnold for maya. https://help.autodesk.com/view/ARNOL/ENU/?guid=arnold_for_maya_displacement_am_Vector_Displacement_html.

[3] Mudbox. vector displacement maps overview. https://download.autodesk.com/us/mudbox/help2011_5/index.html?url=../files/WS73099cc142f487552b5ac6c412649166e6e-6762.htm,topicNumber=d0e21754.

[4] Zbrush. vector displacement maps. <https://help.maxon.net/zbr/en-us/Content/html/user-guide/3d-modeling/exporting-your-model/vector-displacement-maps/vector-displacement-maps.html>. 1

[5] Adobe firefly. <https://www.adobe.com/sensei/generative-ai/firefly.html>. 6

[6] Thimo Alldieck, Gerard Pons-Moll, Christian Theobalt, and Marcus Magnor. Tex2shape: Detailed full human body geometry from a single image. In *Proceedings of the IEEE/CVF International Conference on Computer Vision*, pages 2293–2303, 2019. 2

[7] Melinos Averkiou, Vladimir Kim, Youyi Zheng, and Niloy J. Mitra. Shapesynth: Parameterizing model collections for coupled shape exploration and synthesis. *Computer Graphics Forum (Special issue of Eurographics 2014)*, 2014. 3

[8] Gavin Barill, Nia Dickson, Ryan Schmidt, David I.W. Levin, and Alec Jacobson. Fast winding numbers for soups and clouds. *ACM Transactions on Graphics*, 2018. 5

[9] James F Blinn. Simulation of wrinkled surfaces. In *Seminal graphics: pioneering efforts that shaped the field*, pages 111–117. 1998. 2

[10] Edwin Earl Catmull. *A subdivision algorithm for computer display of curved surfaces*. The University of Utah, 1974. 2

[11] Angel X Chang, Thomas Funkhouser, Leonidas Guibas, Pat Hanrahan, Qixing Huang, Zimo Li, Silvio Savarese, Manolis Savva, Shuran Song, Hao Su, et al. Shapenett: An information-rich 3d model repository. *arXiv preprint arXiv:1512.03012*, 2015. 2

[12] Siddhartha Chaudhuri, Evangelos Kalogerakis, Leonidas Guibas, and Vladlen Koltun. Probabilistic reasoning for assembly-based 3d modeling. *ACM Trans. Graph.*, 30(4), 2011. 3

[13] Siddhartha Chaudhuri, Evangelos Kalogerakis, Stephen Giguere, and Thomas Funkhouser. AttribIt: Content creation with semantic attributes. *ACM Symposium on User Interface Software and Technology (UIST)*, 2013. 3

[14] Yun-Chun Chen, Selena Ling, Zhiqin Chen, Vladimir G. Kim, Matheus Gadelha, and Alec Jacobson. Text-guided controllable mesh refinement for interactive 3d modeling. In *Proceedings of the ACM SIGGRAPH*. ACM, 2024. 5

[15] Zhiqin Chen and Hao Zhang. Learning implicit fields for generative shape modeling. In *Proceedings of the IEEE/CVF conference on computer vision and pattern recognition*, pages 5939–5948, 2019. 2

[16] Christopher B Choy, Danfei Xu, JunYoung Gwak, Kevin Chen, and Silvio Savarese. 3d-r2n2: A unified approach for single and multi-view 3d object reconstruction. In *Computer Vision–ECCV 2016: 14th European Conference, Amsterdam, The Netherlands, October 11–14, 2016, Proceedings, Part VIII 14*, pages 628–644. Springer, 2016. 2

[17] Robert L Cook. Shade trees. In *Proceedings of the 11th annual conference on Computer graphics and interactive techniques*, pages 223–231, 1984. 2

[18] Robert L Cook, Loren Carpenter, and Edwin Catmull. The reyes image rendering architecture. *ACM SIGGRAPH Computer Graphics*, 21(4):95–102, 1987. 2

[19] Matt Deitke, Dustin Schwenk, Jordi Salvador, Luca Weihs, Oscar Michel, Eli VanderBilt, Ludwig Schmidt, Kiana Ehsani, Aniruddha Kembhavi, and Ali Farhadi. Objaverse: A universe of annotated 3d objects. In *Proceedings of the IEEE/CVF Conference on Computer Vision and Pattern Recognition*, pages 13142–13153, 2023. 2, 3, 5

[20] Slava Elizarov, Ciara Rowles, and Simon Donné. Geometry image diffusion: Fast and data-efficient text-to-3d with image-based surface representation. *arXiv preprint arXiv:2409.03718*, 2024. 2

[21] Thomas Funkhouser, Michael Kazhdan, Philip Shilane, Patrick Min, William Kiefer, Ayallet Tal, Szymon Rusinkiewicz, and David Dobkin. Modeling by example. In *ACM SIGGRAPH 2004 Papers*, 2004. 2

[22] Thibault Groueix, Matthew Fisher, Vladimir G Kim, Bryan C Russell, and Mathieu Aubry. A papier-mâché approach to learning 3d surface generation. In *Proceedings of the IEEE conference on computer vision and pattern recognition*, pages 216–224, 2018. 2, 5

[23] Xianfeng Gu, Steven J Gortler, and Hugues Hoppe. Geometry images. In *Proceedings of the 29th annual conference on Computer graphics and interactive techniques*, pages 355–361, 2002. 2

[24] Junlin Han, Filippos Kokkinos, and Philip Torr. Vfusion3d: Learning scalable 3d generative models from video diffusion models. In *European Conference on Computer Vision*, pages 333–350. Springer, 2025. 2, 8

[25] Zexin He and Tengfei Wang. Openlrm: Open-source large reconstruction models. <https://github.com/3DTopia/OpenLRM>, 2023. 6

[26] Paul S Heckbert. Survey of texture mapping. *IEEE computer graphics and applications*, 6(11):56–67, 1986. 2

[27] Yicong Hong, Kai Zhang, Jiuxiang Gu, Sai Bi, Yang Zhou, Difan Liu, Feng Liu, Kalyan Sunkavalli, Trung Bui, and Hao Tan. Lrm: Large reconstruction model for single image to 3d. In *The Twelfth International Conference on Learning Representations*. 2, 4, 6, 7, 8

[28] Arjun Jain, Thorsten Thormählen, Tobias Ritschel, and Hans-Peter Seidel. Exploring shape variations by 3d-model decomposition and part-based recombination. *Comput. Graph. Forum*, 31(2pt3):631–640, 2012. 3

622 [29] Heewoo Jun and Alex Nichol. Shap-e: Generating conditional 3d implicit functions. *arXiv preprint arXiv:2305.02463*, 2023. 2

623 [30] Tomomichi Kaneko, Toshiyuki Takahei, Masahiko Inami, Naoki Kawakami, Yasuyuki Yanagida, Taro Maeda, and Susumu Tachi. Detailed shape representation with parallax mapping. In *Proceedings of ICAT*, pages 205–208, 2001. 2

624 [31] Michael Kazhdan and Hugues Hoppe. Screened poisson surface reconstruction. *ACM Transactions on Graphics (ToG)*, 32(3):1–13, 2013. 5

625 [32] Vladislav Krevoy, Dan Julius, and Alla Sheffer. Model composition from interchangeable components. In *Proceedings of the 15th Pacific Conference on Computer Graphics and Applications*, page 129–138, USA, 2007. IEEE Computer Society. 2

626 [33] Samuli Laine, Janne Hellsten, Tero Karras, Yeongho Seol, Jaakko Lehtinen, and Timo Aila. Modular primitives for high-performance differentiable rendering. *ACM Transactions on Graphics (ToG)*, 39(6):1–14, 2020. 4

627 [34] Jiahao Li, Hao Tan, Kai Zhang, Zexiang Xu, Fujun Luan, Yinghao Xu, Yicong Hong, Kalyan Sunkavalli, Greg Shakhnarovich, and Sai Bi. Instant3d: Fast text-to-3d with sparse-view generation and large reconstruction model. In *The Twelfth International Conference on Learning Representations*. 2, 4

628 [35] Jun Li, Kai Xu, Siddhartha Chaudhuri, Ersin Yumer, Hao Zhang, and Leonidas Guibas. GRASS: Generative recursive autoencoders for shape structures. *ACM Trans. Graphics (Proc. SIGGRAPH)*, 36(4), 2017. 3

629 [36] Minghua Liu, Ruoxi Shi, Linghao Chen, Zhuoyang Zhang, Chao Xu, Xinyue Wei, Hansheng Chen, Chong Zeng, Jiayuan Gu, and Hao Su. One-2-3-45++: Fast single image to 3d objects with consistent multi-view generation and 3d diffusion. In *Proceedings of the IEEE/CVF Conference on Computer Vision and Pattern Recognition*, pages 10072–10083, 2024. 2

630 [37] Minghua Liu, Chao Xu, Haian Jin, Linghao Chen, Mukund Varma T, Zexiang Xu, and Hao Su. One-2-3-45: Any single image to 3d mesh in 45 seconds without per-shape optimization. *Advances in Neural Information Processing Systems*, 36, 2024. 2

631 [38] Ruoshi Liu, Rundi Wu, Basile Van Hoorick, Pavel Tokmakov, Sergey Zakharov, and Carl Vondrick. Zero-1-to-3: Zero-shot one image to 3d object. In *Proceedings of the IEEE/CVF international conference on computer vision*, pages 9298–9309, 2023. 2

632 [39] Yuan Liu, Cheng Lin, Zijiao Zeng, Xiaoxiao Long, Lingjie Liu, Taku Komura, and Wenping Wang. Syncdreamer: Generating multiview-consistent images from a single-view image. In *The Twelfth International Conference on Learning Representations*. 2

633 [40] Xiaoxiao Long, Yuan-Chen Guo, Cheng Lin, Yuan Liu, Zhiyang Dou, Lingjie Liu, Yuexin Ma, Song-Hai Zhang, Marc Habermann, Christian Theobalt, et al. Wonder3d: Single image to 3d using cross-domain diffusion. *CVPR*, 2023. 2, 4, 6, 7, 8

634 [41] Tiange Luo, Chris Rockwell, Honglak Lee, and Justin Johnson. Scalable 3d captioning with pretrained models. *arXiv preprint arXiv:2306.07279*, 2023. 5

635 [42] Tiange Luo, Justin Johnson, and Honglak Lee. View selection for 3d captioning via diffusion ranking. *arXiv preprint arXiv:2404.07984*, 2024. 5

636 [43] Nelson L Max. Horizon mapping: shadows for bump-mapped surfaces. *The Visual Computer*, 4:109–117, 1988. 2

637 [44] Luke Melas-Kyriazi, Iro Laina, Christian Rupprecht, and Andrea Vedaldi. Realfusion: 360deg reconstruction of any object from a single image. In *Proceedings of the IEEE/CVF conference on computer vision and pattern recognition*, pages 8446–8455, 2023. 2

638 [45] Lars Mescheder, Michael Oechsle, Michael Niemeyer, Sebastian Nowozin, and Andreas Geiger. Occupancy networks: Learning 3d reconstruction in function space. In *Proceedings of the IEEE/CVF conference on computer vision and pattern recognition*, pages 4460–4470, 2019. 2

639 [46] Alex Nichol, Heewoo Jun, Prafulla Dhariwal, Pamela Mishkin, and Mark Chen. Point-e: A system for generating 3d point clouds from complex prompts. *arXiv preprint arXiv:2212.08751*, 2022. 2

640 [47] Baptiste Nicolet, Alec Jacobson, and Wenzel Jakob. Large steps in inverse rendering of geometry. *ACM Transactions on Graphics (TOG)*, 40(6):1–13, 2021. 4

641 [48] Patrick Pérez, Michel Gangnet, and Andrew Blake. Poisson image editing. In *Seminal Graphics Papers: Pushing the Boundaries, Volume 2*, pages 577–582. 2023. 5, 6

642 [49] Dustin Podell, Zion English, Kyle Lacey, Andreas Blattmann, Tim Dockhorn, Jonas Müller, Joe Penna, and Robin Rombach. Sdxl: Improving latent diffusion models for high-resolution image synthesis. *arXiv preprint arXiv:2307.01952*, 2023. 2

643 [50] Ben Poole, Ajay Jain, Jonathan T Barron, and Ben Mildenhall. Dreamfusion: Text-to-3d using 2d diffusion. *arXiv preprint arXiv:2209.14988*, 2022. 2, 6

644 [51] Guocheng Qian, Jinjie Mai, Abdullah Hamdi, Jian Ren, Aliaksandr Siarohin, Bing Li, Hsin-Ying Lee, Ivan Skorokhodov, Peter Wonka, Sergey Tulyakov, et al. Magic123: One image to high-quality 3d object generation using both 2d and 3d diffusion priors. *arXiv preprint arXiv:2306.17843*, 2023. 2, 6, 7, 8

645 [52] Alec Radford, Jong Wook Kim, Chris Hallacy, Aditya Ramesh, Gabriel Goh, Sandhini Agarwal, Girish Sastry, Amanda Askell, Pamela Mishkin, Jack Clark, et al. Learning transferable visual models from natural language supervision. In *International Conference on Machine Learning (ICML)*, 2021. 2, 6

646 [53] Robin Rombach, Andreas Blattmann, Dominik Lorenz, Patrick Esser, and Björn Ommer. High-resolution image synthesis with latent diffusion models. In *Proceedings of the IEEE/CVF conference on computer vision and pattern recognition*, pages 10684–10695, 2022. 2, 3

647 [54] Maximilian Seitzer. pytorch-fid: FID Score for PyTorch. <https://github.com/mseitzer/pytorch-fid>, 2020. Version 0.3.0. 2, 6

648 [678] 679 [680] 681 [682] 683 [684] 685 [686] 687 [688] 689 [690] 691 [692] 693 [694] 695 [696] 697 [698] 699 [700] 701 [702] 703 [704] 705 [706] 707 [708] 709 [710] 711 [712] 713 [714] 715 [716] 717 [718] 719 [720] 721 [722] 723 [724] 725 [726] 727 [728] 729 [730] 731 [732] 733 [734]

735 [55] Alla Sheffer, Bruno Levy, Maxim Mogilnitsky, and Alexander Bogomyakov. Abf++: Fast and robust angle based flattening. In *ACM Transactions on Graphics (TOG)*, pages 311–330. ACM, 2005. 4

736 [56] Chao-Hui Shen, Hongbo Fu, Kang Chen, and Shi-Min Hu. Structure recovery by part assembly. *ACM Trans. Graph.*, 31(6), 2012. 3

737 [57] Ruoxi Shi, Hansheng Chen, Zhuoyang Zhang, Minghua Liu, Chao Xu, Xinyue Wei, Linghao Chen, Chong Zeng, and Hao Su. Zero123++: a single image to consistent multi-view diffusion base model. *arXiv preprint arXiv:2310.15110*, 2023. 2, 3

738 [58] Zifan Shi, Sida Peng, Yinghao Xu, Yiyi Liao, and Yujun Shen. Deep generative models on 3d representations: A survey. *CoRR*, abs/2210.15663, 2022. 1

739 [59] Zhengwentai Sun. clip-score: Clip score for pytorch. <https://github.com/taited/clip-score>, 2023. 6

740 [60] Minhyuk Sung, Hao Su, Vladimir G Kim, Siddhartha Chaudhuri, and Leonidas Guibas. ComplementMe: Weakly-supervised component suggestions for 3D modeling. *ACM Transactions on Graphics (TOG)*, 36(6):226, 2017. 3

741 [61] László Szirmay-Kalos and Tamás Umenhoffer. Displacement mapping on the gpu—state of the art. In *Computer graphics forum*, pages 1567–1592. Wiley Online Library, 2008. 2

742 [62] Kenshi Takayama, Ryan Schmidt, Karan Singh, Takeo Igarashi, Tammy Boubekeur, and Olga Sorkine. GeoBrush: Interactive mesh geometry cloning. *Comput. Graph. For. (Proc. EUROGRAPHICS)*, 30(2):613–622, 2011. 3

743 [63] Junshu Tang, Tengfei Wang, Bo Zhang, Ting Zhang, Ran Yi, Lizhuang Ma, and Dong Chen. Make-it-3d: High-fidelity 3d creation from a single image with diffusion prior. In *Proceedings of the IEEE/CVF international conference on computer vision*, pages 22819–22829, 2023. 2

744 [64] Jiaxiang Tang, Zhaoxi Chen, Xiaokang Chen, Tengfei Wang, Gang Zeng, and Ziwei Liu. Lgm: Large multi-view gaussian model for high-resolution 3d content creation. In *European Conference on Computer Vision*, pages 1–18. Springer, 2025. 2, 4

745 [65] Vikram Voleti, Chun-Han Yao, Mark Boss, Adam Letts, David Pankratz, Dmitry Tochilkin, Christian Laforte, Robin Rombach, and Varun Jampani. Sv3d: Novel multi-view synthesis and 3d generation from a single image using latent video diffusion. In *European Conference on Computer Vision*, pages 439–457. Springer, 2025. 2, 8

746 [66] Lifeng Wang, Xi Wang, Xin Tong, Stephen Lin, Shimin Hu, Baining Guo, and Heung-Yeung Shum. View-dependent displacement mapping. *ACM Transactions on graphics (TOG)*, 22(3):334–339, 2003. 2

747 [67] Nanyang Wang, Yinda Zhang, Zhuwen Li, Yanwei Fu, Wei Liu, and Yu-Gang Jiang. Pixel2mesh: Generating 3d mesh models from single rgb images. In *Proceedings of the European conference on computer vision (ECCV)*, pages 52–67, 2018. 2

748 [68] Peng Wang, Hao Tan, Sai Bi, Yinghao Xu, Fujun Luan, Kalyan Sunkavalli, Wenping Wang, Zexiang Xu, and Kai Zhang. Pf-lrm: Pose-free large reconstruction model for joint pose and shape prediction. In *The Twelfth International Conference on Learning Representations*. 2, 4

749 [69] Zhengyi Wang, Cheng Lu, Yikai Wang, Fan Bao, Chongxuan Li, Hang Su, and Jun Zhu. Prolificdreamer: High-fidelity and diverse text-to-3d generation with variational score distillation. *arXiv preprint arXiv:2305.16213*, 2023. 6

750 [70] Zhengyi Wang, Yikai Wang, Yifei Chen, Chendong Xiang, Shuo Chen, Dajiang Yu, Chongxuan Li, Hang Su, and Jun Zhu. Crm: Single image to 3d textured mesh with convolutional reconstruction model. *CoRR*, 2024. 2

751 [71] Daniel Watson, William Chan, Ricardo Martin Bralla, Jonathan Ho, Andrea Tagliasacchi, and Mohammad Norouzi. Novel view synthesis with diffusion models. In *The Eleventh International Conference on Learning Representations*. 2

752 [72] Xinyue Wei, Kai Zhang, Sai Bi, Hao Tan, Fujun Luan, Valentin Deschaintre, Kalyan Sunkavalli, Hao Su, and Zexiang Xu. Meshlrm: Large reconstruction model for high-quality mesh. *arXiv preprint arXiv:2404.12385*, 2024. 2, 4

753 [73] Francis Williams, Teseo Schneider, Claudio Silva, Denis Zorin, Joan Bruna, and Daniele Panozzo. Deep geometric prior for surface reconstruction. In *Proceedings of the IEEE/CVF conference on computer vision and pattern recognition*, pages 10130–10139, 2019. 5

754 [74] Desai Xie, Sai Bi, Zhixin Shu, Kai Zhang, Zexiang Xu, Yi Zhou, Sören Pirk, Arie Kaufman, Xin Sun, and Hao Tan. Lrm-zero: Training large reconstruction models with synthesized data. In *NeurIPS*, 2024. 2

755 [75] Xiaohua Xie, Kai Xu, Niloy J. Mitra, Daniel Cohen-Or, Wenyong Gong, Qi Su, and Baoquan Chen. Sketch-to-design: Context-based part assembly. *Computer Graphics Forum*, xx(xx):xx, 2013. 3

756 [76] Jiale Xu, Weihao Cheng, Yiming Gao, Xintao Wang, Shenghua Gao, and Ying Shan. Instantmesh: Efficient 3d mesh generation from a single image with sparse-view large reconstruction models. *arXiv preprint arXiv:2404.07191*, 2024. 2

757 [77] Kai Xu, Hao Zhang, Daniel Cohen-Or, and Baoquan Chen. Fit and diverse: Set evolution for inspiring 3d shape galleries. *ACM Transactions on Graphics, (Proc. of SIGGRAPH 2012)*, 31(4):57:1–57:10, 2012. 3

758 [78] Qiangeng Xu, Weiyue Wang, Duygu Ceylan, Radomir Mech, and Ulrich Neumann. Dism: Deep implicit surface network for high-quality single-view 3d reconstruction. *Advances in neural information processing systems*, 32, 2019. 2

759 [79] Xingguang Yan, Han-Hung Lee, Ziyu Wan, and Angel X Chang. An object is worth 64x64 pixels: Generating 3d object via image diffusion. *arXiv preprint arXiv:2408.03178*, 2024. 2

760 [80] Haotian Yang, Hao Zhu, Yanru Wang, Mingkai Huang, Qiu Shen, Ruigang Yang, and Xun Cao. Facescape: a large-scale high quality 3d face dataset and detailed riggable 3d face prediction. In *Proceedings of the ieee/cvf conference on computer vision and pattern recognition*, pages 601–610, 2020. 2

761 [792] [793] [794] [795] [796] [797] [798] [799] [800] [801] [802] [803] [804] [805] [806] [807] [808] [809] [810] [811] [812] [813] [814] [815] [816] [817] [818] [819] [820] [821] [822] [823] [824] [825] [826] [827] [828] [829] [830] [831] [832] [833] [834] [835] [836] [837] [838] [839] [840] [841] [842] [843] [844] [845] [846] [847] [848] [849]

850 [81] Lihe Yang, Bingyi Kang, Zilong Huang, Xiaogang Xu, Jiashi
851 Feng, and Hengshuang Zhao. Depth anything: Unleashing
852 the power of large-scale unlabeled data. In *CVPR*, 2024. 2,
853 6, 8

854 [82] Lexing Ying, Aaron Hertzmann, Henning Biermann, and
855 Denis Zorin. Texture and shape synthesis on surfaces. In
856 *Rendering Techniques 2001: Proceedings of the Eurograph-*
857 *ics Workshop in London, United Kingdom, June 25–27, 2001*
858 *12*, pages 301–312. Springer, 2001. 2

859 [83] Alex Yu, Vickie Ye, Matthew Tancik, and Angjoo Kanazawa.
860 pixelnerf: Neural radiance fields from one or few images. In
861 *Proceedings of the IEEE/CVF conference on computer vi-*
862 *sion and pattern recognition*, pages 4578–4587, 2021. 2

863 [84] Dan Zeng, Erin Cahmbers, David Letscher, and Tao Ju. To
864 cut or to fill: a global optimization approach to topologi-
865 cal simplification. *ACM Transactions on Graphics, (Proc. of*
866 *SIGGRAPH 2020)*, 39(6):201:1–201:18, 2020. 4

867 [85] Biao Zhang, Jiapeng Tang, Matthias Niessner, and Peter
868 Wonka. 3dshape2vecset: A 3d shape representation for neu-
869 ral fields and generative diffusion models. *ACM Transactions*
870 *on Graphics (TOG)*, 42(4):1–16, 2023. 2

871 [86] Kai Zhang, Sai Bi, Hao Tan, Yuanbo Xiangli, Nanxuan Zhao,
872 Kalyan Sunkavalli, and Zexiang Xu. Gs-lrm: Large recon-
873 struction model for 3d gaussian splatting. In *European Con-*
874 *ference on Computer Vision*, pages 1–19. Springer, 2025. 2,
875 4

876 [87] Longwen Zhang, Ziyu Wang, Qixuan Zhang, Qiwei Qiu,
877 Anqi Pang, Haoran Jiang, Wei Yang, Lan Xu, and Jingyi Yu.
878 Clay: A controllable large-scale generative model for creat-
879 ing high-quality 3d assets. *ACM Transactions on Graphics*
880 *(TOG)*, 43(4):1–20, 2024. 2

881 [88] Xin-Yang Zheng, Hao Pan, Yu-Xiao Guo, Xin Tong, and
882 Yang Liu. Mvd²: Efficient multiview 3d reconstruction for
883 multiview diffusion. In *ACM SIGGRAPH 2024 Conference*
884 *Papers*, pages 1–11, 2024. 2